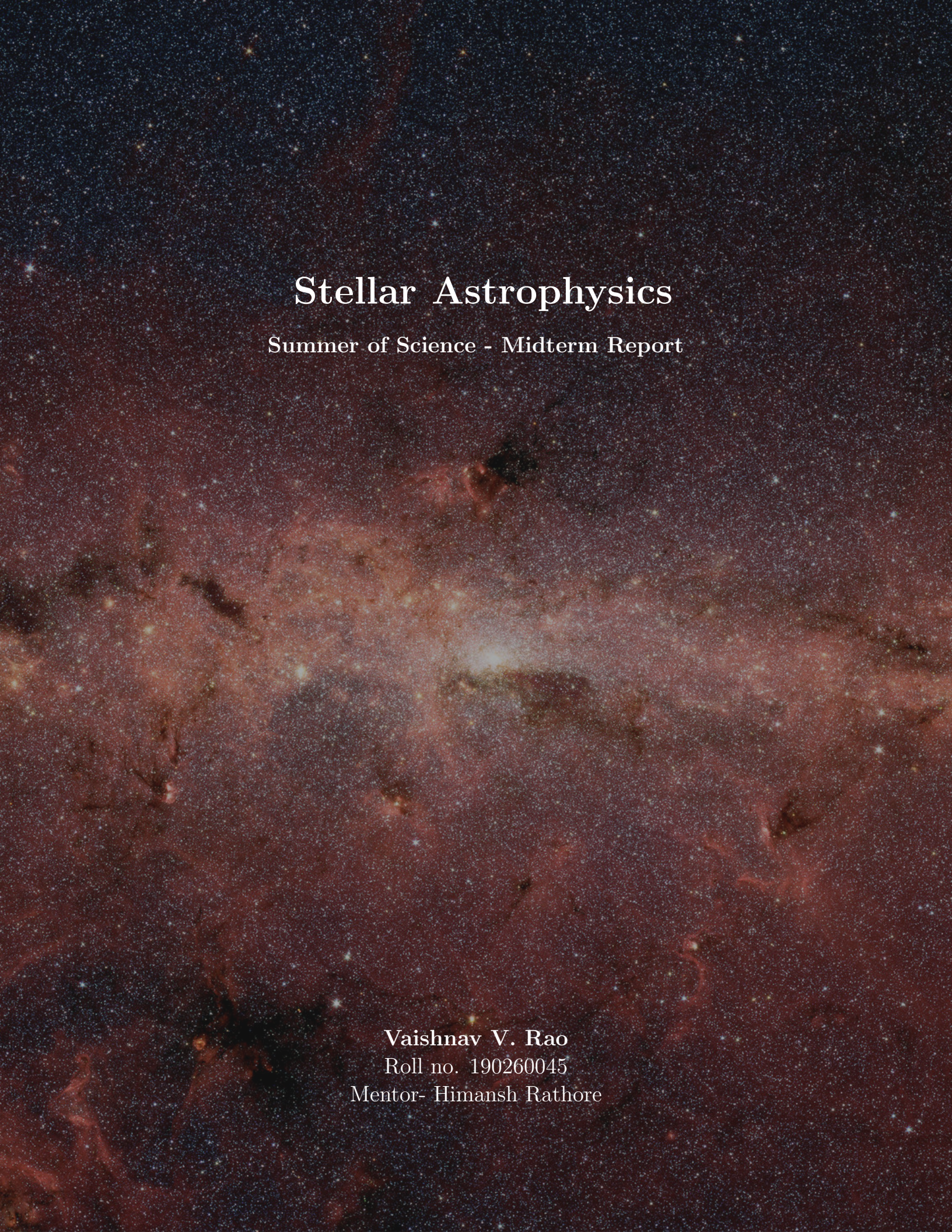

Stellar Astrophysics

Summer of Science - Midterm Report

Vaishnav V. Rao
Roll no. 190260045
Mentor- Himansh Rathore

Contents

1 Introduction

Stellar astrophysics is a subject that deals with understanding the structure, dynamics and evolution of stars through the natural laws of physics with the help of observational astronomy. This subject is considered to be a resounding success of classical and modern physics as theoretical models are in excellent agreement with observed phenomena.

For this midterm report on the course of my study, we will only deal with the stellar structure part of the subject along with some fundamental physics and astronomy topics that act as supplements in our understanding of the subject.

2 Some prerequisites

2.1 The method of trigonometric parallax

Reasonable estimates of the distances to celestial bodies in the Milky Way galaxy (our galaxy) and its local neighbourhood can be made with the method of trigonometric parallax. This method employs the measurement of the angular displacement of the object in question when measured from two points separated by a finite distance. After this, finding the distance to the object is a matter of simple trigonometry provided the finite displacement between the points of measurement is known (Fig 1).

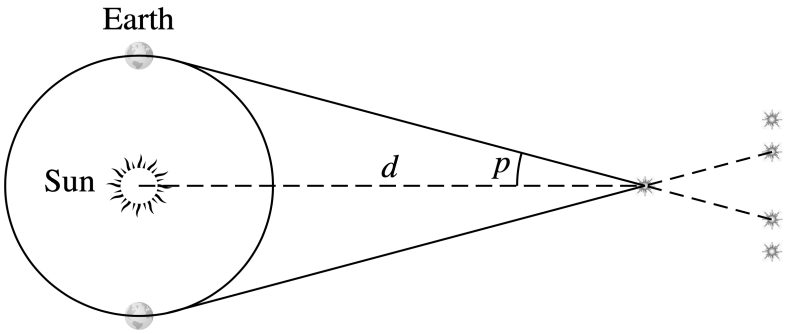

Figure 1: Measurement of parallax angle p [1].

As the distance from the Earth to the Sun is 1 Astronomical Unit (AU),

$$d = \frac{1\text{AU}}{\tan p} \simeq \frac{1}{p}\text{AU}$$

Here, the approximation $\tan p \simeq p$ has been made for parallax angle p measured in *radians*. Alternatively, defining a parsec (parallax-second -pc) to be the distance at which an object subtends 1 *arcsecond*, we have,

$$d = \frac{1}{p''}pc$$

2.2 The Magnitude Scale and more

The radiant flux F measured at a distance r from a star of luminosity L is

$$F = \frac{L}{4\pi r^2} \tag{1}$$

Here we define apparent magnitude m in such a way that a difference of 5 magnitudes between the apparent magnitudes of two stars corresponds to the smaller-magnitude star being 100 times brighter than the larger-magnitude star. Hence,

$$\frac{F_2}{F_1} = 100^{(m_1 - m_2)/5} \tag{2}$$

Absolute magnitude M is defined as the apparent magnitude of the star if it were at a distance of 10 pc from us. Hence, from Eq 1 and 2, we have

$$m - M = 5 \log_{10} \left(\frac{d}{10pc} \right) \tag{3}$$

where d is the distance to the star and $m - M$ is called the distance modulus.

In accordance with Stefan's law, we define effective temperature T_e according to the equation

$$L = 4\pi R^2 \sigma T_e^4 \tag{4}$$

where L is the star's luminosity and R is the star's radius.

2.3 The Theory of Special Relativity

Einstein's theory of Special Relativity stems out of the inability of Galilean Relativity to explain the constancy of speed of light across all inertial frames of reference, in accordance with experiments. The theory itself is based on the following two postulates given by Einstein:

- The Principle of Relativity: The laws of physics are the same in all inertial reference frames.
- The Constancy of the Speed of Light: Light moves through a vacuum at a constant speed c that is independent of the motion of the light source.

A direct consequence of these postulates are the phenomena of length contraction and time dilation.

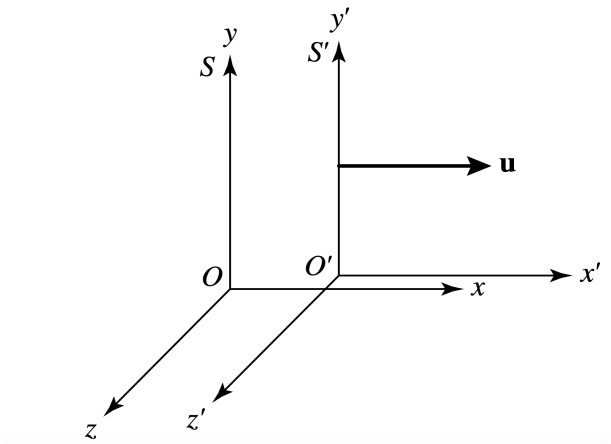

Figure 2: Inertial frames S and $S^{'}$.

2.3.1 Time Dilation & Length Contraction

For two inertial frames of reference S and $S^{'}$ moving with respect to each other as shown above, it is possible to derive the following Lorentz transformation equations using the two postulates and symmetry arguments.

$$\begin{aligned} x' &= \frac{x - ut}{\sqrt{1 - u^2/c^2}} \\ y' = y \quad z' &= z \\ t' &= \frac{t - ux/c^2}{\sqrt{1 - u^2/c^2}} \end{aligned} \tag{5}$$

Here we define the Lorentz factor

$$\gamma = \frac{1}{\sqrt{1 - u^2/c^2}}$$

Suppose light is emitted at intervals of Δt_{rest} at a fixed location in $S^{'}$, then according to Eq. set 5, the time interval Δt_{moving} between successive light emissions as measured form S is

$$\Delta t_{moving} = \gamma \Delta t_{rest} \tag{6}$$

In other words, the time measured from a frame in which the source appears to be moving is *dilated* with respect to the the time measured in the frame in which the source is at rest.

Now, if we consider a rod of length L_{rest} to be at rest in frame $S^{'}$ and make measurements of the positions of the ends of the rod simultaneously from frame S, we get the length of the rod L_{moving} in frame S to be

$$L_{moving} = L_{rest}/\gamma \tag{7}$$

In other words, the length of the rod as measured from a frame in which the rod appears to be moving is *contracted* with respect to the length of the rod measured from the frame in which the rod is at rest.

2.3.2 Relativistic Doppler Effect

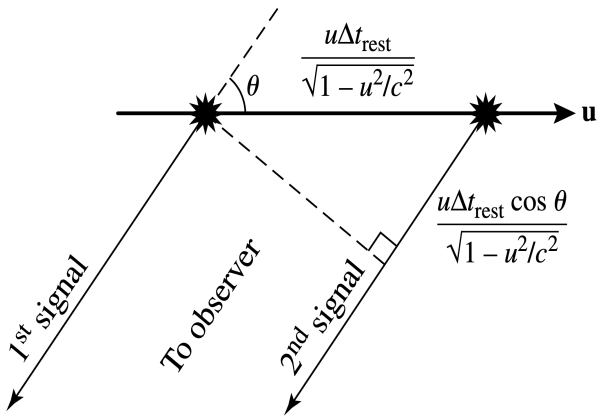

Figure 3: Relativistic Doppler Shift [1].

The above figure shows a source of light moving with a velocity u and emitting light at intervals of Δt_{rest} (frequency $\nu_{rest} = 1/\Delta t_{rest}$) in the frame in which it is at rest. For the special case where $\theta = 0^\circ$ or 180°, we get the observed frequency with which the source is emitting light ν_{obs} as

$$\nu_{obs} = \nu_{rest}\sqrt{\frac{1 - v_r/c}{1 + v_r/c}} \implies \lambda_{obs} = \lambda_{rest}\sqrt{\frac{1 + v_r/c}{1 - v_r/c}} \tag{8}$$

where v_r is the relative speed with which the source is moving *away* from the observer.
From the point of view of astronomy, we also define a redshift parameter

$$z = \frac{\lambda_{obs} - \lambda_{rest}}{\lambda_{rest}} = \frac{\Delta\lambda}{\lambda_{rest}} = \sqrt{\frac{1 + v_r/c}{1 - v_r/c}} - 1 = \frac{\Delta t_{obs}}{\Delta t_{rest}} - 1 \tag{9}$$

2.3.3 Relativistic Momentum and Energy

The relativistic momentum vector $\vec{p}$ of a particle is defined as

$$\vec{p} = \gamma m \vec{v}$$

where $\vec{v}$ is the particle's velocity with respect to the observer and m is the mass of the particle, *invariant* across all frames of reference. From this it is possible to derive the particle's kinetic energy K to be

$$K = mc^2(\gamma - 1)$$

Defining E to be the particle's total relativistic energy γmc^2 we get the following relation from the definition of momentum

$$E^2 = p^2c^2 + m^2c^4 \tag{10}$$

For the special case in which the particle is at rest, we get the famous relation

$$E = mc^2$$

Armed with these tools we will now dive into the realm of astrophysics.

3 Binary systems & Stellar Parameters

Studying astronomy is like reading a detective story. It involves making deductions about a star's size, mass, distance, composition, temperature, velocity, age and a thousand other things by just observing the light coming from it. In this section we see how we can determine the masses and temperatures of stars in binary systems just by making optical observations. But before we get into the detective work, let us see the different kinds of binary systems we shall come across in this section.

- Visual binary: Both stars in the binary can be resolved independently.
- Eclipsing binary: One star periodically passes in front of the other.
- Double-line Spectroscopic binary: Spectral lines of both stars are visible and the spectral lines alternately become single and double about a fixed wavelength λ_o due to the Doppler effect.

3.1 Mass determination using visual binaries

If the distance to a binary star system, whose orbital plane is perpendicular to our line of sight, is known (say using trigonometric parallax), the linear separation of the stars can be determined. From the basic force equations and conservation laws, the ratio of the masses of the stars is

$$\frac{m_1}{m_2} = \frac{r_2}{r_2} = \frac{a_2}{a_1} = \frac{\alpha_2}{\alpha_1} \tag{11}$$

where r_1 and r_2 are the distances of the stars from the centre of mass, a_1 and a_2 are the semi-major axes of the elliptical orbits and α_1 and α_2 are the angles subtended by the semi-major axes (as $\alpha = a/d$, where d is the distance to the binary system)

Kepler's law in general form tells us:

$$T^2 = \frac{4\pi^2 a^3}{G(m_1 + m_2)} \tag{12}$$

where $a = a_1 + a_2$. Thus if a can be determined, the individual masses of the stars can be determined using Eq. 11. Further, if the plane of the ellipses is inclined at an angle i to the plane of the sky, we have

$$\begin{aligned} m_1 + m_2 &= \frac{4\pi^2(\alpha d)^3}{GT^2} = \frac{4\pi^2}{G}\left(\frac{d}{\cos i}\right)^3 \frac{\tilde{\alpha}^3}{T^2} \\ \frac{m_1}{m_2} &= \frac{\alpha_2}{\alpha_1} = \frac{\tilde{\alpha_2}\cos i}{\tilde{\alpha_1}\cos i} = \frac{\tilde{\alpha_2}}{\tilde{\alpha_1}} \end{aligned} \tag{13}$$

where $\tilde{\alpha} = \tilde{\alpha_1} + \tilde{\alpha_2}$, the observed angles subtended by the semi-major axes.

3.2 Eclipsing Spectroscopic Binaries

3.2.1 Variation of velocity

For double-line spectroscopic binary systems, the radial velocities of the two stars can be determined through Doppler shifts. If we assume the orbits to be circular and the orbital plane to be in the line of sight ($i = 90°$), the measured radial velocities of the two stars will be sinusoidal. For the cases $i \neq 90°$, the maximum measured radial velocities will be scaled by a factor of $\sin i$ and the radial velocities themselves will remain sinusoidal but lesser in amplitude. If the orbits are elliptical, the observed radial velocity curves become skewed and non-sinusoidal.

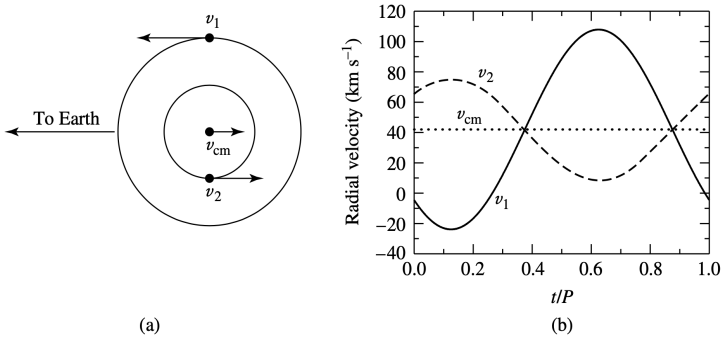

Figure 4: The orbital paths and radial velocities of two stars in circular orbits. (a)The plane of the orbits lie along the line of sight of observer. (b) The observed radial velocity curves [1].

3.2.2 Mass Function

If the eccentricity of the elliptical orbits $e << 1$, the orbital speeds are almost constant. Hence, $v_1 = 2\pi a_1/T$ and $v_2 = 2\pi a_2/T$. Thus from Eq. 11, we have

$$\frac{m_1}{m_2} = \frac{v_2}{v_1} = \frac{v_{2r}/\sin i}{v_{1r}/\sin i} = \frac{v_{2r}}{v_{1r}} \tag{14}$$

where v_{1r} and v_{2r} are the observed radial velocities. Now, $a = a_1 + a_2 = T/2\pi(v_1 + v_2)$. Using this in Eq. 12,

$$m_1 + m_2 = \frac{T(v_{1r} + v_{2r})^3}{2\pi G \sin^3 i}$$

For single line spectroscopic binaries, say star 1 is observable and star 2 is not. This means only v_{1r} is measurable. Using the above two equations we arrive at

$$\frac{m_2^3}{(m_1 + m_2)^2} \sin^3 i = \frac{T}{2\pi G} v_{1r}^3 \tag{15}$$

The term on the RHS is called mass function as it is a function of readily observable quantities. If either m_1 or i is unknown, the mass function sets a lower limit for m_2 as the LHS is always lesser than m_2.

3.2.3 Using eclipses to find radii and ratio of temperatures

If a binary star system is observed to be an eclipsing binary, it is reasonable to take $i \approx 90°$. Further the radii of these stars can be determined by using the duration of these eclipses and the radial velocities of the stars. The following figure illustrates this

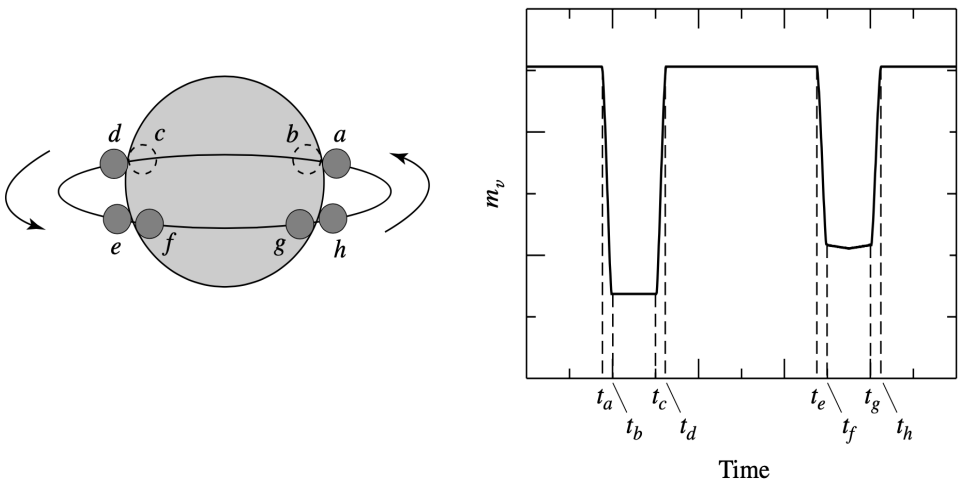

Figure 5: The light curve for an eclipsing binary with $i \approx 90°$. The times indicated on the light curve correspond to the positions of the smaller star relative to it's larger companion. It is assumed that the smaller star is hotter [1].

Assuming $a_s >> r_s, r_l$ (the radii of the smaller and larger star), we have

$$\begin{aligned} r_s &= v/2(t_b - t_a) \\ r_l &= v/2(t_c - t_a) \end{aligned} \tag{16}$$

where $v = v_s + v_l$ is the relative velocity of one star with respect to the other (orbital speeds are typically non relativistic).

The ratio of temperatures of eclipsing binaries can also be determined from the light curves. We know that the radiative surface flux is given by $F_r = \sigma T_e^4$ from Eq. 1. Thus the amount of light detected when both the stars are visible is given by

$$B_0 = k(\pi r_l^2 F_{rl} + \pi r_s^2 F_{rs}) \tag{17}$$

where k is a constant that is dependent on the distance to the system and the nature of the detector. Similarly, the amount of light detected during the primary minima of the light curve (when the smaller star is behind) and the secondary minima (when the smaller star is in front) is

$$\begin{aligned} B_p &= k\pi r_l^2 F_{rl} \\ B_s &= k(\pi r_l^2 - \pi r_s^2)F_{rl} + k\pi r_s^2 F_{rs} \end{aligned} \tag{18}$$

Since it is not possible to determine k, ratios are employed.

$$\frac{B_0 - B_p}{B_0 - B_s} = \frac{F_{rs}}{F_{rl}} = \left(\frac{T_s}{T_l}\right)^4 \tag{19}$$

A notable thing to mention at this point is that extraterrestrial planets have been discovered by observing the dimming of starlight caused by the transit of planets in front of their parent stars. Another method of detecting extraterrestrial planets is measuring the radial velocity variations of the parent star induced by the *gravitational tug* of the planet. To get an idea of just how unbelievably small these variations can be, the radial velocity variation of the Sun due to Jupiter is roughly 12 m/s. Similar to the speed of a world class sprinter from Earth!

4 Classification of Stellar Spectra

4.1 The Harvard Classification of Stellar Spectra

Spectral Type	Temperature (Kelvin)	Spectral Lines
O	28,000 - 50,000	Ionized helium
B	10,000 - 28,000	Helium, some hydrogen
A	7500 - 10,000	Strong hydrogen, some ionized metals
F	6000 - 7500	Hydrogen, ionized calcium (labeled H and K on spectra) and iron
G	5000 - 6000	Neutral and ionized metals, especially calcium; strong G band
K	3500 - 5000	Neutral metals, sodium
M	2500 - 3500	Strong titanium oxide, very strong sodium

Figure 6: The table above shows some characteristic emission and absorption lines of each type of star [2].

4.2 Some Statistical Physics

Stellar classification is based on the fact that different spectral lines have different strengths at different temperatures. We now aim to explain this phenomenon through statistical physics. In this section we take the the case of the Balmer absorption line.

We know that the no. of gas particles per unit volume having speeds between v and $v + dv$ is given by the Maxwell-Boltzmann Distribution.

$$n_v dv = n\left(\frac{m}{2\pi kT}\right)^{3/2} e^{-mv^2/2kT} 4\pi v^2 dv \tag{20}$$

where n = total no. density and $n_v = \partial n/\partial v$.

The atoms of a gas gain and lose energy through collisions. As a result, the distribution in the speeds of impacting atoms produces a definite distribution of electrons among the atomic orbitals. Let s_a be a specific set of quantum no.s that identifies a state of energy E_a for a system of particles. The ratio of the probability $P(s_b)$ that the system is in state s_b to the probability $P(s_a)$ that the system is in state s_a is given by the Boltzmann equation.

$$\frac{P(s_b)}{P(s_a)} = \frac{e^{-E_b/kT}}{e^{-E_a/kT}} = e^{-(E_b - E_a)/kT} \tag{21}$$

Now, we define g_a and g_b to be the no. of states with energies E_a and E_b respectively (statistical weights). Then, the ratio of probabilities of finding an atom having energies E_b and E_a in the system is

$$\frac{P(E_b)}{P(E_a)} = \frac{g_b e^{-E_b/kT}}{g_a e^{-E_a/kT}} = \frac{g_b}{g_a} e^{-(E_b - E_a)/kT} = \frac{N_b}{N_a} \tag{22}$$

which is also the ratio of no. of atoms N_b and N_a (in different states of excitation) having energies E_b and E_a.

Applying only the Boltzmann equation to a gas of neutral hydrogen atoms where equal no. of atoms occupy the ground and first excited states, we get a temperature of around 85,000 K. This means that for a significant no. of atoms to occupy the first excited state, very high temperatures are required. But, as observations reveal, Balmer absorption line intensities peak at much lower temperatures of around 9,500 K. The answer to this discrepancy lies in considering the relative no. of atoms in different stages of *ionization*. The Saha equation gives us this relative no.
We define a partition function

$$Z_i = \sum_{j=1}^{\infty} g_j e^{-(E_j - E_i)/kT}$$

For all further considerations, $i = 1$ is taken to be the non-ionised stage.
Now, the ratio of no. of atoms in ionisation stage $i + 1$ to no. of atoms in ionisation stage i is

$$\frac{N_{i+1}}{N_i} = \frac{2Z_{i+1}}{n_e Z_i}\left(\frac{2\pi m_e kT}{h^2}\right)^{3/2} e^{-\chi_i/kT} \tag{23}$$

where χ_i is the ionization energy needed to remove an electron from an atom or ion (in the ground state) thus taking it from ionisation stage i to ionisation stage $i + 1$. n_e is the free electron no.

density.
Before combining the Saha and Boltzmann equations, we familiarise ourselves with the following terms:
N_I: no. of non-ionised hydrogen atoms
N_1: no. of hydrogen atoms in ground state
N_{II}: no. of singly ionised hydrogen atoms
N_2: no. of hydrogen atoms in 1^{st} excited state

The strength of the Balmer absorption line depends on the ratio N_2/N_{total} i.e the fraction of *all* hydrogen atoms in the first excited state. At this point we make the reasonable approximation $N_1 + N_2 \simeq N_I$ and write

$$\frac{N_2}{N_{total}} = \left(\frac{N_2}{N_1 + N_2}\right)\left(\frac{N_I}{N_{total}}\right) = \left(\frac{N_2/N_1}{1 + N_2/N_1}\right)\left(\frac{1}{1 + N_{II}/N_I}\right) \tag{24}$$

The individual ratios in the above equation can be found out using the Saha and Boltzmann equations. This equation can be thought of as the probability of finding the atom unionised *and* in the first excited state.

Now, if we plot N_2/N_{total} as a function of temperature after substituting the necessary values for the partition function, ionisation energy, and free electron density in a typical star, we get a maxima at approximately 9900 K in good agreement with observations.

4.3 H-R Diagrams

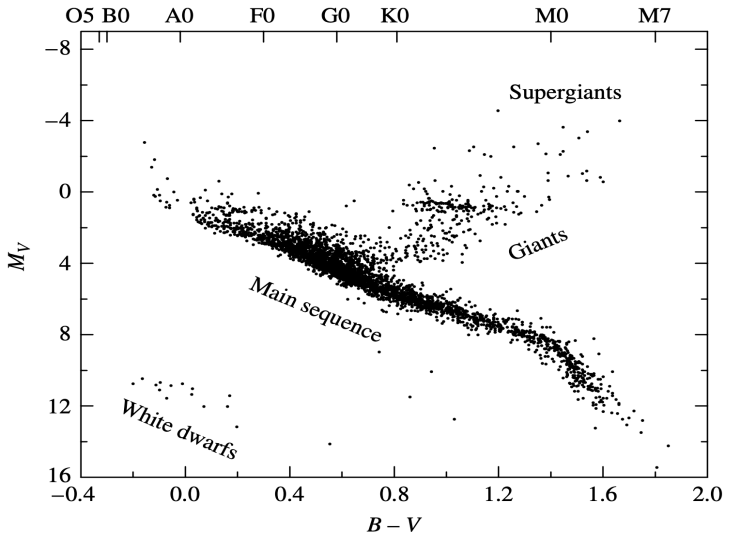

Figure 7: An observer's HR Diagram with data from the Hipparcos catalog [1].

A HR Diagram is a scatter plot of a star's absolute magnitude/luminosity vs. temperature/spectral class. In the above HR diagram, luminosity increases on moving up (as a lower magnitude implies higher luminosity) and temperature decreases on moving to the right. If two stars are of the same spectral type (approximately same effective temperature), a higher luminosity implies that the star

is larger (from Eq 4). Thus, the groups in the HR Diagram have been labelled accordingly. With such a simple relation between temperature and luminosity, the position of the star on the main sequence is totally determined by the *mass* of the star, with mass increasing as we move up the main sequence.

Another question that arises is whether there is a difference in the spectra of giant and main sequence stars of the same spectral type. The answer is yes! It is found that for stars of the same spectral type, narrower spectral lines are produced by more luminous stars. This is the basis for the Morgan-Keenan luminosity classes.

Class	Type of Star
Ia-O	Extreme, luminous supergiants
Ia	Luminous supergiants
Ib	Less luminous supergiants
II	Bright giants
III	Normal giants
IV	Subgiants
V	Main-sequence (dwarf) stars
VI, sd	Subdwarfs
D	White dwarfs

Figure 8: The Morgan-Keenan luminosity classes [1].

These roman numerals are appended to the Harvard stellar classification of a star. Using both the types of stellar classification, the exact position of a star on the HR Diagram can now be determined by just reading the spectra of the star. The diagram itself is an important tool for finding the distances to stars by the method of main-sequence matching.

5 Stellar Atmospheres

The light that astronomers receive from a star comes from the star's atmosphere, the layers of gas overlying the opaque interior. The temperature, density, and composition of the atmospheric layers from which these photons escape determine the features of the star's spectrum. To interpret the observed spectral lines properly, we must describe how light travels through the gas that makes up a star.

5.1 The Radiation Field

5.1.1 Specific and Mean Intensities

$E_\lambda d\lambda$ is assumed to be the amount of energy that rays with wavelengths in between λ and $\lambda + d\lambda$, emerging form a surface dA, carry into the cone in a time dt as shown in figure 14. Here, $E_\lambda = \partial E/\partial\lambda$. With this, the specific intensity of the rays is defined as

$$I_\lambda = \frac{\partial I}{\partial \lambda} = \frac{E_\lambda d\lambda}{d\lambda\, dt\, dA \cos\theta\, d\Omega} \tag{25}$$

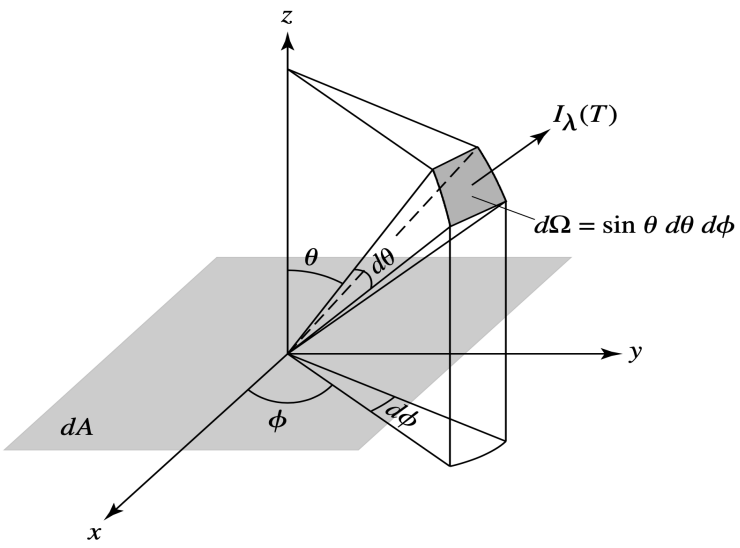

Figure 9: Intensity I_λ [1].

Here, I_λ is defined in the limit $d\Omega \to 0$. Which means I_λ does not spread out and intensity of such a ray remains constant as it travels through empty space.
The mean intensity is the specific intensity averaged over all directions.

$$\langle I_\lambda \rangle = \frac{1}{4\pi} \int I_\lambda d\lambda = \frac{1}{4\pi} \int_{\phi=0}^{2\pi} \int_{\theta=0}^{\pi} I_\lambda \sin\theta \, d\theta \, d\phi \tag{26}$$

For an isotropic radiation field like black body radiation $\langle I_\lambda \rangle = B_\lambda$ (the Planck Function).

5.1.2 Specific Energy density, Radiative Flux and Radiation Pressure

The energy per unit volume in a radiation field having a wavelength between λ and $\lambda + d\lambda$ is

$$u_\lambda d\lambda = \frac{4\pi}{c} \langle I_\lambda \rangle d\lambda \tag{27}$$

Specific radiative flux is the net energy having a wavelength between λ and $\lambda + d\lambda$ that passes each second through a unit area int z-direction.

$$F_\lambda d\lambda = \int I_\lambda d\lambda \cos\theta \, d\Omega = \int_{\phi=0}^{2\pi} \int_{\theta=0}^{\pi} I_\lambda d\lambda \cos\theta \sin\theta \, d\theta \, d\phi \tag{28}$$

For an isotropic radiation field, $F_\lambda = 0$ as there is no net transport of energy.
For a resolved source, what we measure as intensity, is the specific intensity, but for an unresolved source, what is being measured is the specific radiative flux.

It can also be derived that the specific radiation pressure of a photon 'gas' is given by

$$P_{rad,\lambda} = \frac{1}{c} \int_{sphere} I_\lambda d\lambda \, \cos^2\theta \, d\Omega = \frac{4\pi}{3c} I_\lambda d\lambda \text{ for isotropic radiation} \tag{29}$$

5.2 Stellar Opacity

5.2.1 Definition of opacity

The change in intensity dI_λ of a light ray of wavelength λ as it passes through a gas, on account of absorption and scattering, is proportional to the intensity of the light ray, density of the gas and the distance ds travelled through it. Thus,

$$dI_\lambda = -\kappa_\lambda \rho I_\lambda ds \tag{30}$$

where κ_λ is the wavelength dependent absorption coefficient or opacity. The above equation can be integrated from some fixed reference point to get

$$I_\lambda = I_{\lambda,0} e^{-\int_0^s \kappa_\lambda \rho \, ds} \tag{31}$$

The characteristic distance travelled by a photon before being removed from the beam is taken to be

$$l = \frac{1}{\kappa_\lambda \rho} \tag{32}$$

5.2.2 Optical depth

For scattered photons, the characteristic distance l is in fact the mean free path of the photons, an expression which can be derived from statistical physics.

$$l = \frac{1}{\kappa_\lambda \rho} = \frac{1}{n\sigma_\lambda} \tag{33}$$

We now define wavelength dependent optical depth τ_λ, back along a light ray as follows:

$$d\tau_\lambda = -\kappa_\lambda \rho \, ds \tag{34}$$

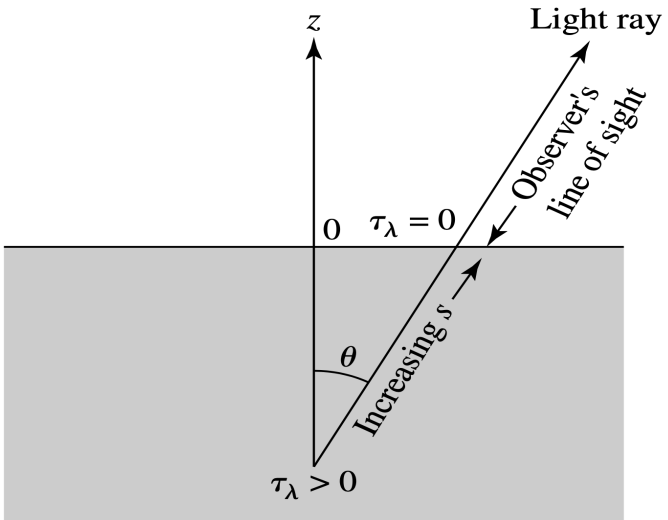

Figure 10: Optical depth τ_{lambda} measured back along a ray's path [1].

We can take the outermost layer of the star to be taken at optical depth $\tau_\lambda = 0$ after which light travels unimpeded to the observer. The optical depth may be thought of as the no. of mean free paths from the original position to the surface as measured along the ray's path. As a result we typically see no deeper into an atmosphere at a given wavelength then $\tau_\lambda \approx 1$.

It is often useful to employ an opacity that has been averaged over all wavelengths so as to get an opacity that only depends on the composition, density and temperature. The most commonly used mean is the Rosseland Mean Opacity.

$$\frac{1}{\bar{\kappa}} = \frac{\int_0^\infty \frac{1}{\kappa_\nu}\frac{\partial B_\nu(T)}{\partial T}d\nu}{\int_0^\infty \frac{\partial B_\nu(T)}{\partial T}d\nu} \tag{35}$$

5.3 Transfer equation and Radiation Pressure gradient

If we consider absorption, emission *and* scattering, the change in intensity of a light ray as it travels a distance ds through the atmosphere is given by the transfer equation

$$\begin{aligned} dI_\lambda &= -\kappa_\lambda I_\lambda ds + j_\lambda \rho\, ds \\ \implies \frac{dI_\lambda}{d\tau_\lambda} &= I_\lambda - S_\lambda \end{aligned} \tag{36}$$

where $S_\lambda = j_\lambda/\kappa_\lambda$ is called the source function.
If we make the assumption that the atmosphere is plane parallel, and gray (opacity does not depend on wavelength), replace I_λ and S_λ with I and S integrated over all wavelengths, and replace τ with τ_v, the vertical optical depth with the necessary scaling factor of $1/\cos\theta$ as in figure 14, we get the following form of the transfer equation:

$$\cos\theta \frac{dI}{d\tau_v} = I - S \tag{37}$$

which can be integrated over all solid angles or multiplied by $\cos\theta$ and integrated over all solid angles to get the following two equations from equations 28 and 29.

$$\begin{aligned} \frac{dF_{rad}}{d\tau_v} &= 4\pi(\langle I\rangle - \langle S\rangle) \\ \frac{dP_{rad}}{dr} &= -\frac{\bar{\kappa}\rho}{c} F_{rad} \end{aligned}$$

For equilibrium stellar atmospheres, $F_{rad} = const. = F_{surf} = \sigma T_e^4$. Thus the second equation can be integrated to get radiation pressure as a function of optical depth.

$$P_{rad} = \frac{1}{c} F_{rad}\tau_v + C \tag{38}$$

5.4 Eddington Approximation

If we knew how the radiation pressure varied with temperature for the general case we can use Eq. 38 to get a temperature profile of our plane-parallel, gray atmosphere. The Eddington approximation allows us to do just that. According to this, the intensity of radiation is assigned one value I_{out} in the $+z$ direction and I_{in} in the $-z$ direction. Here both I_{out} and I_{in} vary with depth and I_{in}

is taken to be zero at the surface where τ_v is zero. After working out the consequences of this approximation through the previous equations, it can be shown that

$$S = \langle I \rangle = \frac{3\,\sigma\,T_e^4}{4\,\pi}\left(\tau_v + \frac{2}{3}\right) \tag{39}$$

If we further assume that the atmosphere is in Local Thermodynamic Equilibrium, we get

$$T^4 = \frac{3}{4}\,T_e^4\left(\tau_v + \frac{2}{3}\right) \tag{40}$$

which is the required temperature profile.
This equation tells us that the "surface" of a star, which by definition has temperature T_e, is not at the top of the atmosphere, where $\tau_v = 0$, but deeper down, where $\tau_v = 2/3$. This result may be thought of as the average point of origin of the observed photons. Thus, when looking at a star, we see down to a vertical optical depth of $\tau_v \approx 2/3$, averaged over the disk of the star.

5.5 Limb Darkening

It is observed that the *limbs* of stars are darker and less luminous compared to the centre of the star. We now aim to explain this phenomenon.
The second form of the transfer equation from equation group 36, can be multiplied with $e^{-\tau_\lambda}$ and integrated from origin of the ray to top of the atmosphere to get emergent intensity $I_\lambda(0)$ as

$$I_\lambda(0) = I_{\lambda,0}e^{-\tau_{\lambda,0}} - \int_{\tau_{\lambda,0}}^{0} S_\lambda e^{-\tau_\lambda} d\tau_\lambda \tag{41}$$

where $I_{\lambda,0}$ is the initial intensity. Now, if we make the assumption of a plane parallel atmosphere and replace τ_λ with $\tau_{v,\lambda}$, take initial position of the rays to be at $\tau_{v,0} = \infty$ and drop the λ subscripts for simplicity, we get

$$I(0) = \int_0^\infty S \sec\theta\; e^{-\tau_v \sec\theta} d\tau_v \tag{42}$$

If we assume $S = a + b\tau_v$, then the above equation takes the form

$$I_\lambda(0) = a_\lambda + b_\lambda \cos\theta \tag{43}$$

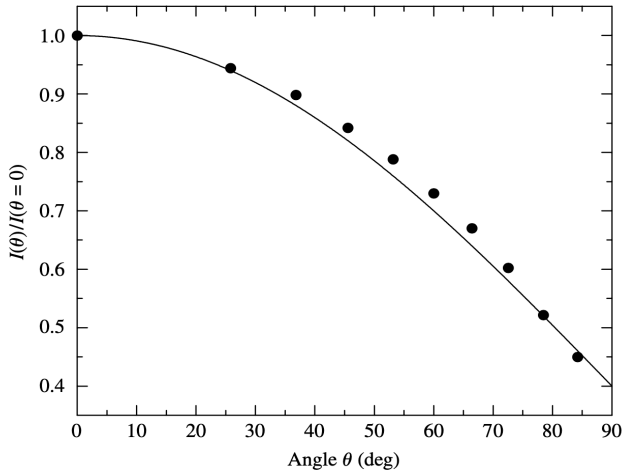

Figure 11: A theoretical Eddington approximation of solar limb darkening for light integrated over all wavelengths. The dots are observational data for the Sun [1].

If we use the Eddington approximation and the result we obtained in Eq. 39 and solve for the Sun we get a pretty close match with the observational data obtained for the Sun as shown in the figure above.

6 The Sun

Due to its proximity to us, the star for which we have the greatest amount of observational data is our Sun. The tremendous wealth of information provided by the data serve as rigorous tests of our understanding of the physical processes operating within stellar atmospheres and interiors. In this section we will only go into the solar neutrino problem, the Parker solar wind model, the hydrodynamic nature of the upper solar atmosphere, magnetohydrodynamics and the solar cycle.

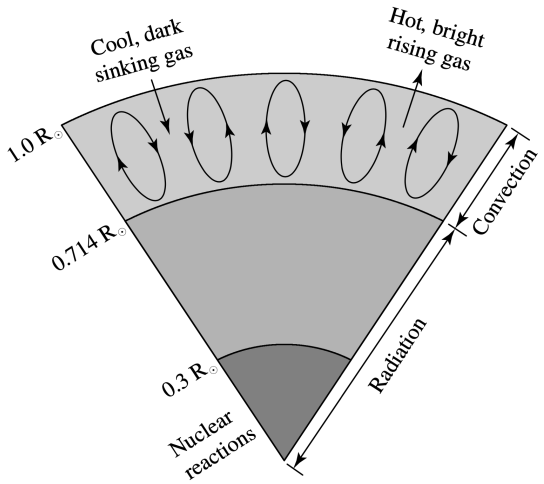

Figure 12: Schematic diagram of the Sun's interior [1].

6.1 The Solar Neutrino Problem

Neutrinos are produced in different stages of the pp chain reaction in the solar interior. A discrepancy existed for decades between the predicted values of neutrino counts that should be detected on Earth, based on the solar model, and the actual neutrino counts that were detected by various neutrino observatories around the world. The actual neutrino counts were always significantly lesser than the predicted values.

The only logical explanation to this was either the solar model was fundamentally wrong or something was happening to the neutrinos on their way to Earth. An elegant solution to the solar neutrino problem proposed that the solar model is essentially correct but that the neutrinos produced in the Sun's core actually change before they reach Earth. The Mikheyev–Smirnov–Wolfenstein (or MSW) effect involves the transformation of neutrinos from one type to another.

The neutrinos produced in the various branches of the pp chain are all electron neutrinos (ν_e); however, two other flavors of neutrinos also exist—the muon neutrino (ν_μ) and the tau neutrino (ν_τ). The MSW effect suggests that neutrinos oscillate among flavors, being electron neutrinos, muon neutrinos, and/or tau neutrinos during their passage through the Sun. The neutrino oscillations are caused by interactions with electrons as the neutrinos travel toward the surface

6.2 The Parker Solar Wind Model

This model assumes that the solar corona is in hydrostatic equilibrium, is isothermal and has a negligible mass compared to the mass of the sun. With this, the condition for hydrostatic equilibrium gives us

$$\frac{dP}{dr} = -\frac{GM_\odot \rho}{r^2} \tag{44}$$

where $M_\odot$ is the mass of the Sun. If we assume all of the gas to be made up of hydrogen which is completely ionised, take no. density as $n = \rho/m_p$ and $m_p \approx m_n$, we get

$$P = 2nkT \tag{45}$$

according to the ideal gas law, where $\mu = 1/2$ for ionised hydrogen.
Combining the above two equations and integrating, we get

$$n(r) = n_0 e^{-\lambda(1-r_0/r)} \tag{46}$$

where

$$\lambda \equiv \frac{GM_\odot n\, m_p}{2kTr_0}$$

which can also be written as

$$P(r) = P_0 e^{-\lambda(1-r_0/r)} \tag{47}$$

where P_0 is the pressure at some r_0.

Plugging in the necessary constants in the equation and calculating $P(\infty)$, we get $P(\infty) \simeq 5 \times 10^{-6}$. However, with the exception of localized clouds of material, the actual densities and pressures of interstellar dust and gas are much lower than those just derived. As the assumption about the corona being isothermal is roughly consistent with observations, the assumption that the solar corona is in hydrostatic equilibrium must be wrong. Since $P(\infty)$ greatly exceeds the pressures in interstellar space, material must be expanding outward from the Sun, implying the existence of the solar wind.

The existence of the solar wind has an important implication. As the Sun rotates and the solar wind ejects mass outward, there is a net torque opposing the rotation. The solar wind transfers angular momentum away from the Sun, slowing down its speed of rotation.

6.3 Hydrodynamic nature of the upper solar atmosphere

The following hydrodynamic equations help us in describing the outer atmosphere, as it is not in hydrostatic equilibrium.

$$\rho v \frac{dv}{dr} = -\frac{dP}{dr} = -\frac{GM_r \rho}{r^2} \tag{48}$$

where M_r is the mass that is enclosed by a sphere of radius r. Based on the fact that loss rate of mass is constant, we also have

$$4\pi r^2 \rho v = const \implies \frac{d}{dr}\left(\rho v r^2\right) = 0 \tag{49}$$

At the top of the convection zone, rising and falling gas sets up longitudinal waves (pressure waves) that propagate outward through the photosphere and the chromosphere.

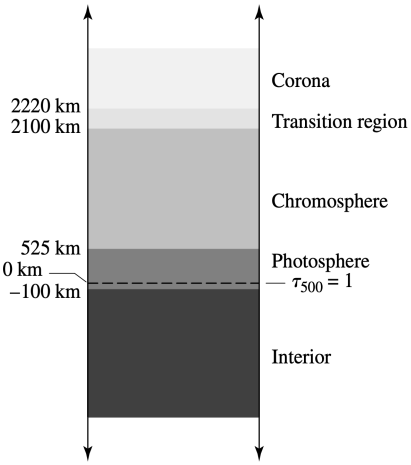

Figure 13: The components of the Sun's atmosphere [1].

The outward flux of wave energy F_E, is governed by the equation

$$F_E = \frac{1}{2}\rho v_w^2 v_s \tag{50}$$

where v_s is the local sound speed and v_w is the velocity amplitude of the oscillatory wave motion for individual particles being driven about their equilibrium positions by the "piston" of the convection zone.

$$v_s = \sqrt{\frac{\gamma P}{\rho}} = \sqrt{\frac{\gamma kT}{\mu m_H}} \propto \sqrt{T} \tag{51}$$

From photosphere to chromosphere, T does not change much. Hence v_s is almost the same. If we assume negligible loss of mechanical energy ($F_E(4\pi r^2) = constant$), a significant drop in ρ means v_w has to increase according to Eq. 50. When $v_w > v_s$, the waves become supersonic, causing shockwaves that dissipate energy in the chromosphere. Through this mechanism, the upper layers of the Sun's atmosphere get heated up due to convection in the interior.

6.4 Magnetohydrodynamics (MHD) and Alfvén waves

The magnetic energy density u_m and magnetic pressure P_m are numerically equal and are given by

$$u_m = \frac{B^2}{2\mu_0} = P_m \tag{52}$$

Now, if a volume V of plasma containing a number of magnetic field lines is compressed perpendicular to the lines, the density of field lines necessarily increases. Hence, magnetic energy increases by an amount equal to the external work done. This also means that there is a magnetic pressure developed which works to counteract the displacement caused. This is the "restoring force" that can set up oscillations and waves in the medium. These transverse MHD waves that are set up are called Alfvén waves.

The speed of propagation of the Alfvén wave may be estimated by making a comparison with the sound speed in a gas. Hence,

$$v_m \sim \sqrt{\frac{P_m}{\rho}} = \frac{B}{\sqrt{2\mu_0\rho}} \tag{53}$$

But, a more careful treatment gives

$$v_m = \frac{B}{\mu_0 \rho} \tag{54}$$

According to Maxwell's equations, a time-varying magnetic field produces an electric field, which in turn creates electrical currents in the highly conductive plasma. This implies that some resistive Joule heating will occur in the ionised gas due to Alfv en waves, causing the temperature to rise. Thus MHD waves contribute to the temperature structure of the upper solar atmosphere.

6.5 The Solar Cycle

The overall magnetic field of the Sun reverses every 11 years. This is linked with the sunspot cycle which also shows 11 year patterns.

6.5.1 Sunspots

Sunspots occur in regions of very high magnetic field strengths with the magnetic field lines themselves coming out of the surface of the Sun. It is believed that the existence of such intense magnetic fields "freezes" the plasma in the convection zone, inhibiting the energy transport outward, explaining why sunspots appear dark.

As part of the cycle which lasts 22 years, the sunspots first appear in higher latitudes and then start appearing at lower and lower latitudes until they meet at the equator (a period of around 11 years). Each sunspot lasts for a few months and is of the opposite polarity as the one preceding it. Following this there is a global magnetic field reversal of the Sun and the next sunspot that again appears at the higher latitude is of opposite polarity to the first sunspot that had appeared there 11 years ago. Thus a cycle of about 22 years is established.

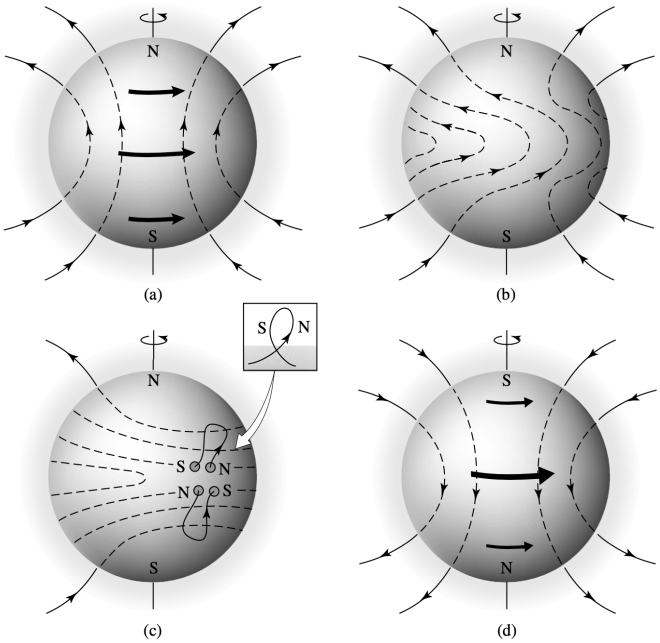

Figure 14: The Magnetic dynamo model of the Solar Cycle [1].

6.5.2 The Magnetic Dynamo Model

As depicted in the figure above, because the magnetic field lines are "frozen into" the gas, the differential rotation of the Sun drags the lines along, converting a poloidal field (essentially a simple magnetic dipole) to one that has a significant toroidal component (field lines that are wrapped around the Sun). The turbulent convection zone then has the effect of twisting the lines, creating regions of intense magnetic fields, called magnetic ropes. The buoyancy produced by magnetic pressure (Eq. 53) causes the ropes to rise to the surface, appearing as sunspot groups. The polarity of the sunspots is due to the direction of the magnetic field along the ropes; consequently, every lead spot in one hemisphere will have the same polarity while the lead spots in the other hemisphere will have the opposite polarity. Finally, the cancellation of magnetic fields near the equator causes the poloidal field to be reestablished, but with its original polarity reversed. This process takes approximately 11 years.

7 Plan of Action

- Finish up the remainder of Stellar Structure by reading the chapter *Interior of Stars* from the main reference book and finish said chapter by 7^{th} May.
- Read the chapter *Star Formation* from the same book.
- Get into Stellar Dynamics and Evolution by reading chapters 13 through 16 from the main reference book and finish it by 31^{st} May.

References

[1] Bradley W. Carroll, Dale A. Ostlie. *An Introduction to Modern Astrophysics.* Pearson, 2014.

[2] *Sloan Digital Sky Survey/ Sky Server* http://cas.sdss.org/dr7/en/proj/advanced/spectraltypes/lines.asp